Structural mechanism for versatile cargo recognition by the yeast class V myosin Myo2

Received for publication, January 14, 2019, and in revised form, February 14, 2019 Published, Papers in Press, February 25, 2019, DOI 10.1074/jbc.RA119.007550

Kun Tang[‡1], **Yujie Li**[‡], **Cong Yu**[‡§], **and Zhiyi Wei**[‡2]

From the [‡]*Department of Biology, Southern University of Science and Technology, Shenzhen 518055 and the* [§]*Guangdong Provincial Key Laboratory of Cell Microenvironment and Disease Research, Shenzhen Key Laboratory of Cell Microenvironment, Shenzhen, China 518055*

Edited by Wolfgang Peti

Class V myosins are actin-dependent motors, which recognize numerous cellular cargos mainly via the C-terminal globular tail domain (GTD). Myo2, a yeast class V myosin, can transport a broad range of organelles. However, little is known about the capacity of Myo2-GTD to recognize such a diverse array of cargos specifically at the molecular level. Here, we solved crystal structures of Myo2-GTD (at 1.9–3.1 Å resolutions) in complex with three cargo adaptor proteins: Smy1 (for polarization of secretory vesicles), Inp2 (for peroxisome transport), and Mmr1 (for mitochondria transport). The structures of Smy1- and Inp2-bound Myo2-GTD, along with site-directed mutagenesis experiments, revealed a binding site in subdomain-I having a hydrophobic groove with high flexibility enabling Myo2-GTD to accommodate different protein sequences. The Myo2-GTD-Mmr1 complex structure confirmed and complemented a previously identified mitochondrion/vacuole-specific binding region. Moreover, differences between the conformations and locations of cargo-binding sites identified here for Myo2 and those reported for mammalian MyoVA (MyoVA) suggest that class V myosins potentially have co-evolved with their specific cargos. Our structural and biochemical analysis not only uncovers a molecular mechanism that explains the diverse cargo recognition by Myo2-GTD, but also provides structural information useful for future functional studies of class V myosins in cargo transport.

Class V myosins have long been recognized as key molecular motors involved in intracellular transport along actin filaments. Mammals contain three class V myosins, MyoVa/b/c, whereas the budding yeast *Saccharomyces cerevisiae* has two, Myo2 and Myo4. All of these are composed of an N-terminal motor domain followed by six IQ motifs, a central coiled-coil (CC)[3] region, and a C-terminal globular tail domain (GTD, also called cargo-binding domain or CBD) (1–3) (Fig. 1*A*). As unconventional myosins, class V myosins possess an amazing ability to recognize numerous cargos, such as various organelles, vesicles, protein complexes, and even mRNA (4–6). The selection, recognition, and binding of those cargoes mainly rely on the GTDs of class V myosins (5, 7–10).

Myo2 is the major player in the transport of organelles in budding yeasts (11). During the budding process, Myo2 directionally delivers organelles from the mother cell to the bud tip in an efficient way. The GTD of Myo2 (Myo2-GTD) was found to be responsible for recognizing a broad array of cargo adaptor proteins in *S. cerevisiae* (1). So far, a dozen cargo adaptors have been well characterized to directly interact with Myo2-GTD in cargo loading and transport, including mitochondria receptor Myo2 receptor-related protein 1 (Mmr1) (12, 13), vacuole-related protein Vac17 (14, 15), inheritance of peroxisomes gene 2 (Inp2) (16–18), and also as Rab GTPase family proteins, Sec4, Ypt32, and Ypt11 (19–21). Additionally, a kinesin-like protein Smy1 (suppressor of myosin) was shown to bind with Myo2-GTD and cooperate with Sec4 in the secretory vesicle transport (22–25).

Previous mutagenesis studies suggested some key amino acids as potential cargo-binding sites for transporting mitochondria, vacuoles, and secretory vesicles (26) (Fig. 1*B*). However, for a long time only the apo-structure of Myo2-GTD was solved (10). Therefore the molecular mechanisms underlying the various cargo recognitions by Myo2-GTD remain elusive. Recently, several structures of MyoVa-GTD in complex with cargos were solved. Considering the significant differences in the GTD structures between MyoVa and Myo2 (Fig. 1*B*), and the fact that most cargo adaptors of Myo2 have no homologues in mammals, transferring the knowledge gained from the cargo-bound structures of mammalian MyoVa to yeast Myo2 would be difficult.

In this study, we determined crystal structures of Myo2-GTD in complex with three cargo adaptor proteins, Mmr1, Smy1,

This work was supported by the National Natural Science Foundation of China Grants 31770791 and 31570741 (to Z. W.), 31600612 (to K. T.), and 31870757 (to C. Y.), Natural Science Foundation of Guangdong Province Grant 2016A030312016, Science and Technology Planning Project of Guangdong Province Grant 2017B030301018, Shenzhen Science and Technology Innovation Commission Grants JCYJ20160229153100269 and ZDSYS20140509142721429, and the Recruitment Program of Global Youth Experts of China (to Z. W. and C. Y.). The authors declare that they have no conflicts of interest with the contents of this article.

This article contains Figs. S1–S9.

The atomic coordinates and structure factors (codes 6IXO, 6IXP, 6IXQ, and 6IXR) have been deposited in the Protein Data Bank (http://wwpdb.org/).

[1] To whom correspondence may be addressed. E-mail: tangk@sustc.edu.cn.

[2] Member of the Neural and Cognitive Sciences Research Center, SUSTech. To whom correspondence may be addressed. Tel.: 86-88018411; E-mail: weizy@sustc.edu.cn.

[3] The abbreviations used are: CC, coiled-coil; GTD, globular tail domain; Mmr1, mitochondrial Myo2 receptor-related 1; Inp2, inheritance of peroxisomes gene 2; Smy1, suppressor of myosin; MIS, Myo2-interacting site; TEV, tobacco etch Virus; ITC, isothermal titration calorimetry; PDB, Protein Data Bank; r.m.s., root mean square.

and Inp2. These complex structures reveal two independent binding sites in Myo2-GTD. One of the sites for interaction with Mmr1 was consistent with the previously reported mitochondrion/vacuole-specific binding region. Importantly, the other binding site identified for both Smy1 and Inp2 is a novel cargo-binding site in Myo2-GTD. This new site exhibits major structural differences between vertebrate MyoVa and Myo2, suggesting it may be specific to yeast myosin V. Moreover, the conformational flexibility of the Smy1/Inp2-binding site allows different cargo recognition in an overlapping site, providing a mechanistic explanation of the diversified cargo recognition by Myo2.

Results

Modification of Myo2-GTD for crystallization

To explore Myo2-GTD–mediated cargo recognition, we systematically studied the interaction between GTD and reported binding partners. First, we successfully expressed and purified the C-terminal GTD of Myo2, comprising residues 1087–1574, in a bacterial expression system. To crystallize the GTD/cargo complexes, limited trypsin digestion was applied to treat the GTD sample as previously reported (10, 27). However, the trace amount of residual protease was observed to digest the highly flexible binding targets (Fig. S1*A*), and thereby to disrupt the complex formation. To solve this problem, we designed a new GTD construct (GTDΔL) by removing a flexible N-terminal loop (residues 1087–1151) and a central loop (residues 1342–1347), which contains a potential trypsin-cleavage site (27) (Fig. 1*A*). Such a modification did not impair the binding of Myo2 to its binding partner, Mmr1 (Fig. S1*B*), but promoted crystallization in many screen conditions without the trypsin treatment. We determined the Myo2-GTDΔL structure at 1.9 Å resolution (Table 1). GTDΔL adopts the same conformation as the previously reported apo-structure (10) with an overall r.m.s. deviation of 0.9 Å. Therefore, we used GTDΔL for the following structural and biochemical characterizations.

The GTDΔL structure contains two α-helical subdomains (Fig. 1*B*). In subdomain-I, the N terminus and C terminus are packed together by the interaction between α1 and α16. Such a conformation is largely different from the corresponding regions of MyoVa (Fig. 1*B*). Another significant structural difference has been found at the α6/α7 region. Compared with MyoVa-GTD, the α6 and α7 helices in Myo2-GTD are much longer. These different structural elements in subdomain-I together with α4 and a long loop connecting subdomains-I and -II (loop-I/II) create a groove unique to Myo2-GTD (Fig. 1*B* and Fig. S2).

Smy1 occupies a hydrophobic groove in Myo2-GTD

As the binding site for Smy1 on Myo2-GTD is still unknown, we chose Smy1 as our first target for uncovering the cargo recognition mechanisms of GTD. Smy1 was first reported to be a kinesin-like protein, which suppresses a temperature-sensitive phenotype of cells carrying a motility-deficient mutation in Myo2 (22, 28). By interacting with both actin and Myo2, Smy1 enhances the motility of Myo2 (29) and cooperates with Sec4 in transporting secretory vesicles (24). The Myo2-interacting site

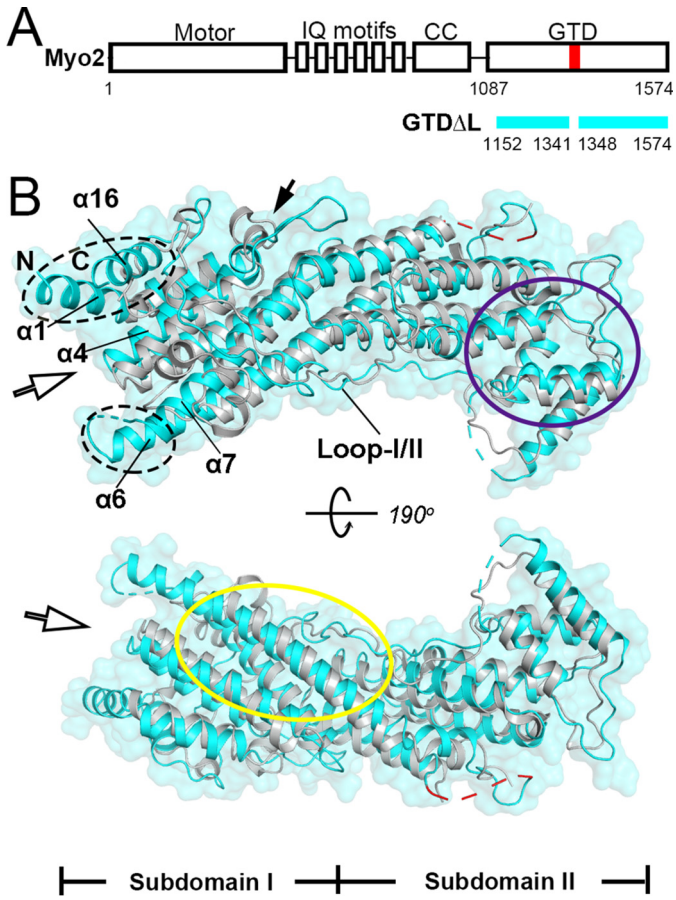

Figure 1. Structural characterization of Myo2-GTD. *A,* schematic diagram showing the domain organization of yeast Myo2. The GTDΔL construct with the deleted potential trypsin cleavage sequence (*red*) was used in this study. *B,* structural comparison of the Myo2-GTDΔL (cyan) and MyoVa-GTD (*gray*, PDB code 3WB8) (9) with an overall r.m.s. deviation of 2.2 Å. The two regions specific for the binding of Myo2 to mitochondrion/vacuole and to vesicle are indicated by *yellow* and *purple circles*, respectively. The structural differences are indicated by *black arrows* and *dashed circles*. The two protrusions highlighted by *dashed circles* in Myo2-GTD form a unique groove that does not exist in MyoVa-GTD.

(MIS) in Smy1 was mapped onto its C-terminal region (25) (Fig. 2*A*).

Consistent with the previous result, the quantitative analysis using isothermal titration calorimetry (ITC) indicated that Smy1-MIS (residues 564–656) interacts with Myo2-GTDΔL with a binding affinity of ~3 μM (Fig. S3). To understand how Myo2 can specifically recognize Smy1, we aimed to solve the Myo2-GTDΔL/Smy1-MIS complex by protein crystallography. However, extensive crystallization trials failed to yield any complex crystals presumably due to the highly flexible nature of MIS. To overcome this problem, we split the MIS sequence into two halves based on the sequence analysis: a highly conserved C-terminal half (Smy1-MIS^{C}, residues 615–650) and a less conserved N-terminal half (Smy1-MIS^{N}, 564–614). Because Smy1-MIS^{C} showed a moderate binding affinity of ~20 μM to GTDΔL, whereas Smy1-MIS^{N} did not bind with GTDΔL (Fig. 2 and Fig. S3), we used the Smy1-MIS^{C} protein for the complex preparation with GTDΔL. To avoid the dissociation between Smy1-MIS^{C} and GTDΔL during purification, we covalently linked the two fragments together as a chimera (Smy1-MIS^{C}::GTDΔL) by fusing the Smy1-MIS^{C} sequence to the N

Table 1
Statistics of data collection and model refinement
Numbers in parentheses represent the value for the highest resolution shell.

Dataset	GTD	GTD/Smy1	GTD/Inp2	GTD/Mmr1
Data collection				
Space group	$P2_12_12_1$	$P3_221$	$P3_221$	$C2$
Unit cell parameters				
a, b, c (Å)	50.7, 72.2, 168.3	93.5, 93.5, 204.1	63.5, 63.5, 225.8	110.4, 63.5, 169.1
α, β, γ (°)	90, 90, 90	90, 90, 120	90, 90, 120	90, 104.7, 90
Resolution range (Å)	50–1.9 (1.93–1.9)	50–3.06 (3.22–3.06)	50–2.85 (3.01–2.85)	50–2.73 (2.88–2.73)
No. of unique reflections	49,545 (2,455)	20,270 (2,911)	13,042 (1,854)	28,335 (4,404)
Redundancy	11.6 (12.1)	18.7 (20.7)	19.0 (20.1)	6.8 (7.2)
I/σ	23.5 (1.6)	20.9 (2.5)	14.5 (2.5)	8.1 (2.8)
Completeness (%)	100 (100)	99.7 (100)	99.9 (99.8)	93.4 (99.6)
R_{merge} (%)[a]	10.6 (190.5)	6.7 (165.6)	17.0 (153.2)	8.7 (106.9)
$CC_{1/2}$	0.993 (0.764)	0.998 (0.978)	0.998 (0.963)	0.999 (0.927)
Structure refinement				
Resolution (Å)	50–1.9 (1.95–1.9)	50–3.06 (3.22–3.06)	50–2.85 (3.07–2.85)	50–2.73 (2.84–2.73)
R_{cryst}/R_{free} (%)[b]	17.4 (30.9)/20.6 (36.2)	20.3 (35.7)/22.3 (39.4)	20.9 (35.3)/26.3 (40.9)	24.2 (37.5)/28.3 (42.5)
R.m.s. deviations				
Bonds (Å)	0.014	0.004	0.002	0.003
Angles (°)	1.3	0.6	0.5	0.7
Average B factor	48.7	172.9	93.4	106.1
No. of atoms				
Protein atoms	3,151	3,258	3,212	6,792
Ligand/ion	21	0	10	0
Water molecules	256	0	0	4
Ramachandran plot				
Favored regions (%)	97.9	96.5	96.7	97.0
Allowed regions (%)	2.1	3.5	3.3	3.0
Outliner (%)	0	0	0	0

[a] $R_{merge} = \Sigma|I_i - I_m|/\Sigma I_i$, where I_i is the intensity of the measured reflection and I_m is the mean intensity of all symmetry related reflections.
[b] $R_{cryst} = \Sigma||F_{obs}| - |F_{calc}||/\Sigma|F_{obs}|$, where F_{obs} and F_{calc} are observed and calculated structure factors. $R_{free} = \Sigma_T||F_{obs}| - |F_{calc}||/\Sigma_T|F_{obs}|$, where T is a test data set of about 5% of the total reflections randomly chosen and set aside prior to refinement.

terminus of GTDΔL connected by a tobacco etch virus (TEV) cutting site. Afterward, TEV protease was added to the purified sample during crystallization. By using this strategy, we successfully obtained complex crystals and solved the crystal structure of the Myo2-GTDΔL/Smy1-MIS^C complex at a resolution of 3.06 Å using the molecular replacement method (Table 1).

In the complex structure, the peptide (residues 633–647) containing 15 residues of Smy1-MIS^C can be clearly assigned (Fig. S4*A*). The Smy1-MIS^C peptide occupies the Myo2-unique groove in subdomain-I, burying ~800 Å^2 of solvent-accessible surface area (Fig. 2*C*), which was not previously recognized as a cargo-binding site. To tightly hold Smy1-MIS^C, the groove adopts a hand-like conformation. In the complex structure, α6, α7, and a helix (αA) between them together form a "thumb," α1 and α16 are "fingers," whereas α4 and the C-terminal part of the loop-I/II act as a "palm." The groove is largely hydrophobic with hydrophobic residues in the groove clustered into two patches. The first hydrophobic patch, mainly formed by aromatic residues from the thumb and palm (*e.g.* W1213$_{Myo2}$, F1261$_{Myo2}$, F1264$_{Myo2}$, F1275$_{Myo2}$, Y1287$_{Myo2}$, F1542$_{Myo2}$), recognizes L637$_{Smy1}$ and L639$_{Smy1}$ in the N-terminal part of Smy1-MIS^C (Fig. 2*D*). The second hydrophobic patch, formed by smaller residues from the fingers and the palm (*e.g.* I1207$_{Myo2}$, V1545$_{Myo2}$, V1565$_{Myo2}$, A1566$_{Myo2}$, V1569$_{Myo2}$, V1570$_{Myo2}$), interacts with I642$_{Smy1}$ and V644$_{Smy1}$ in the C-terminal part of Smy1-MIS^C (Fig. 2*D*).

Consistently, disruption of the hydrophobic interactions by mutating L637$_{Smy1}$, L639$_{Smy1}$, or I642$_{Smy1}$ to a charged residue (glutamic acid) abolishes the Myo2-GTDΔL/Smy1-MIS^C interaction (Fig. 2*B*). Likewise, the F1264E or F1275E mutation in the hydrophobic groove of Myo2 dramatically weakens the binding of Myo2-GTDΔL to Smy1-MIS^C (Table 2). In contrast, mutations in the mitochondrion/vacuole-specific binding site, away from the Smy1-binding groove, show little effects on the binding (Table 2). Indeed, previous yeast two-hybrid assay of truncation mutants of Myo2-GTD indicated that deletion of the C-terminal α16 finger is sufficient to eliminate its binding to Smy1 (10). In addition to the hydrophobic interactions, the binding of Smy1-MIS^C to GTDΔL is strengthened by hydrogen bonds, which help fixing the backbone conformation of Smy1-MIS^C and positioning the residues, such as L637$_{Smy1}$, L639$_{Smy1}$, and I642$_{Smy1}$, with their side chains facing to the hydrophobic groove of Myo2-GTDΔL (Fig. 2*D*). The interacting residues in either Smy1 or Myo2 are highly conserved across various budding species (Fig. 2*A* and Fig. S2), suggesting that the Smy1-mediated vesicle transport of Myo2 is very likely a common feature of budding yeasts.

Inp2 possesses a similar GTD binding mode to Smy1

Given the large number of known cargos for Myo2, it was important to probe whether the Smy1-binding groove in GTD could accommodate cargo proteins other than Smy1. Because the Myo2/Smy1 interaction requires the three highly conserved residues (Leu-637, Leu-639, and Ile-642) in MIS^C (Fig. 2, *A* and *B*), a (L/F)*XLXX*(I/V/L) sequence pattern found in other cargo proteins, where *X* denotes any of the 20 common amino acids, may use the similar GTD-binding mode. To test our hypothesis, we first searched the sequence pattern from previously identified cargo proteins by using the SCANSITE server. Interestingly, Inp2, which is a peroxisome-specific receptor for Myo2 (17), was found to have the above sequence pattern in the middle of the peptide sequence (residues 531–543) (Fig. 3*A*). In line with our findings, this highly conserved region (Inp2-MIS)

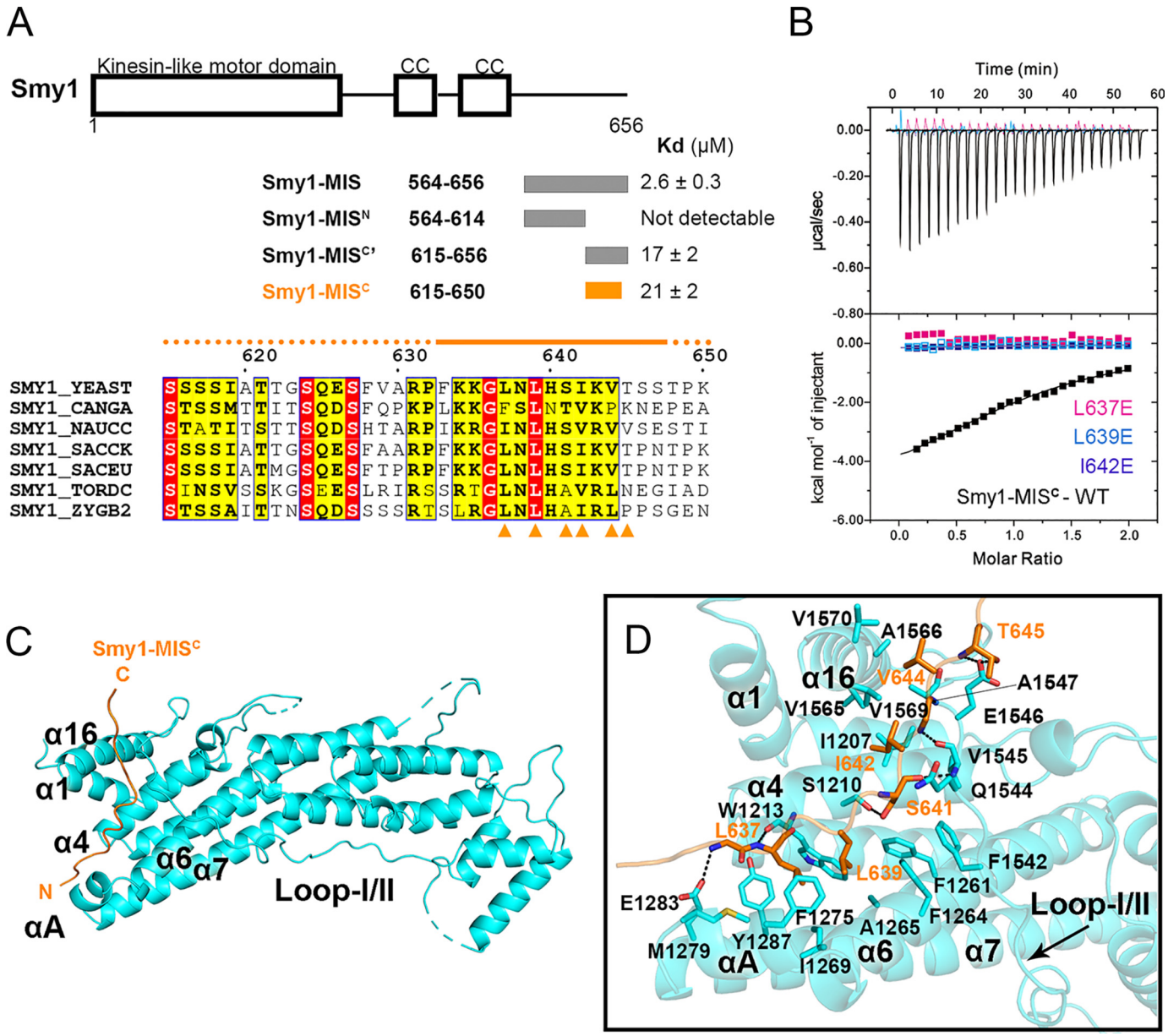

Figure 2. The Smy1-MIS/Myo2-GTDΔL interaction. *A,* characterization of Smy1, the Myo2 cargo adaptor for vesicle transport. The schematic diagram shows the domain organization of Smy1 and the Smy1-MIS truncation constructs used in this study. K_d values of the binding of these Smy1 constructs to Myo2-GTDΔL were measured by using ITC-based analysis. The sequence alignment was shown for the MIS^C regions of the Smy1 proteins from different yeast species: YEAST, *S. cerevisiae*; CANGA, *Candida glabrata*; NAUCC, *Naumovozyma castellii*; SACCK, *Saccharomyces kudriavzevii*; SACEU, *Saccharomyces eubayanus*; TORDC, *Torulaspora delbrueckii*; ZYGB2, *Zygosaccharomyces bailii*. Residues identical or highly similar are shown in *red* and *yellow boxes*, respectively. The ordered and disordered loops of the Smy1-MIS^C peptide in the complex structure were indicated *above* the alignment by *solid and dotted lines*, respectively. Residues involved in the interaction with GTD are indicated by *triangles*. *B,* ITC-based analysis of the binding of Smy1-MIS^C and its variants to Myo2-GTDΔL. *C,* the overall structure of Smy1-MIS^C bound Myo2-GTDΔL. *D,* interface details. Hydrogen bonds and salt bridges are indicated by *dashed lines*.

Table 2
Summary of K_d values (μM) measured by ITC-based analysis

		Smy1-MIS^C	Inp2-MIS	Mmr1-MIS^C	Vac17-MIS
	GTDΔ-WT	21 ± 2	32 ± 9	6.8 ± 1.1	0.35 ± 0.02
Smy1/Inp2-binding mutations	Smy1-MIS^C::GTDΔL	Not detectable	Not detectable	6.2 ± 0.4	0.39 ± 0.04
	GTDΔL-E1211A	–[a]	–	6.4 ± 0.9	0.31 ± 0.05
	GTDΔL-F1264E	>100	Not detectable	–	–
	GTDΔL-F1275E	>200	Not detectable	11.3 ± 3.7	0.35 ± 0.07
Mitochondrial-binding mutations	GTDΔL-D1297N	14 ± 2	–	21 ± 2	Not detectable
	GTDΔL-Y1303A	14 ± 2	–	Not detectable	Not detectable
	GTDΔL-K1311E	20 ± 4	–	Not detectable	0.18 ± 0.01
	GTDΔL-K1312A	19 ± 4	–	Not detectable	0.50 ± 0.04

[a] Dash represents not determined. The corresponding titration curves can be found in Fig. S5.

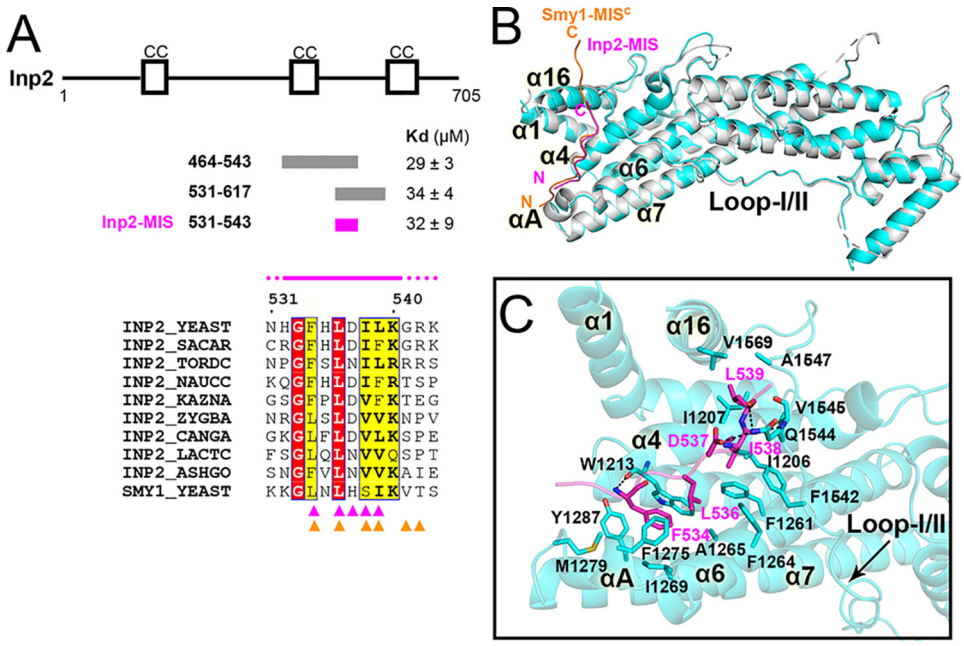

Figure 3. The Inp2-MIS/Myo2-GTDΔL interaction. *A,* characterization of Inp2, the Myo2 cargo adaptor for peroxisome positioning. The presentation style of *A* follows that of Fig. 2*A*. In the sequence alignment of Inp2-MIS, additional species were added: SACAR, *Saccharomyces arboricola*; KAZNA, *Kazachstania naganishii*; ZYGBA, *Z. bailii*; LACTC, *Lachancea thermotolerans*; ASHGO, *Ashbya gossypii*. In addition, the Smy1-MIS^C sequence was also aligned to the Inp2-MIS sequences. Residues involved in the binding of Inp2-MIS and Smy1-MIS^C to Myo2-GTDΔL are indicated by *magenta* and *orange triangles*, respectively. *B,* the overall structure of Inp2-MIS bound Myo2-GTDΔL. The structure of Smy1-MIS^C/GTDΔL complex was superimposed for comparison. *C*, interface details.

falls in a Inp2 fragment reported to interact with Myo2-GTD (17).

Next, ITC was employed to test the potential interaction between Inp2-MIS and Myo2-GTDΔL. The results indicate that Inp2-MIS directly interacts with GTDΔL with a relatively low binding affinity of ~30 μM (Fig. 3*A*), and neither an extension at the N-terminal or C-terminal end of the Inp2 would significantly increase the binding affinity (Fig. 3*A* and Fig. S6). By applying the similar strategy that we used for crystallization of the Myo2-GTDΔL/Smy1-MIS^C complex, we succeeded in solving the Myo2-GTDΔL/Inp2-MIS complex structure at 2.85 Å resolution (Table 1).

Fully consistent with our prediction, the Inp2-MIS peptide also binds to the hydrophobic groove in subdomain-I of Myo2-GTD (Fig. 3*B*). Although only nine residues (residues 532–540, Fig. S4*B*) were clearly assigned in the structure, the short Inp2-MIS peptide adopts a similar conformation to Smy1-MIS^C (Fig. 3*B*). In detail, three highly conserved hydrophobic residues (Phe-534, Leu-536, and Leu-539) in Inp2-MIS reside in the same positions as the corresponding residues in Smy1-MIS^C and form hydrophobic interactions with Myo2-GTDΔL (Fig. 3, *A* and *C*). Besides, Ile-538 in Inp2-MIS is also involved in the hydrophobic interactions. Similarly to the Myo2/Smy1 interaction, several hydrogen bonds that are mainly formed between the side chains of Myo2-GTDΔL and the main chains of Inp2-MIS further enhance the Myo2/Inp2 interaction. To validate our structure, because the Inp2-binding site was reported to locate at subdomain-II of Myo2-GTD (18), we measured the binding of the cargo proteins to the Smy1-MIS^C::GTDΔL fusion protein, in which Smy1-MIS^C is covalently linked to the N terminus of GTDΔL and presumably covers the Smy1/Inp2-binding groove. Our results indicate that neither Inp2-MIS nor Smy1-MIS^C show a detectable binding to the fusion protein (Table 2), thus confirming our structural findings.

Mmr1 interacts with the mitochondrion/vacuole-specific binding site of GTD via both hydrophobic and charge–charge interactions

Genetic studies indicate that Myo2 is required for Mmr1-mediated mitochondrial distribution (12, 13, 26, 30, 31). Additionally, using yeast two-hybrid and co-immunoprecipitation assays, Eves *et al.* (26) revealed that a region containing residues 398–430 in Mmr1 is necessary and sufficient for the binding of Mmr1 to Myo2-GTD (Fig. 4*A*). By performing analytical gel filtration and ITC-based binding assays, we confirmed that this region of Mmr1 and Myo2-GTD forms a 1:1 complex with binding affinity of ~7 μM (Figs. S1*B* and S7). Moreover, we found that including an additional ~40–50 residues in the N terminus of the reported Myo2-interacting site increases the binding affinity ~3-fold (Fig. 4, *A* and *B*). Thus, we named these N-terminal extensions and the original boundaries as Mmr1-MIS (residues 349–430), Mmr1-MIS′ (residues 360–430), and Mmr1-MIS^C (residues 398–430), respectively. The three Mmr1 boundaries were screened for crystallization with Myo2-GTDΔL and only the Mmr1-MIS^C and GTDΔL mixture could be crystallized. The structure of the Myo2-GTDΔL/Mmr1-MIS^C complex was determined at 2.73 Å resolution (Table 1). Each asymmetric unit contains two essentially identical complexes. To our surprise, in one complex, two Mmr1-MIS^C molecules were found to interact with GTDΔL at two different sites (Fig. 4*C* and Fig. S4, *C* and *D*).

As shown in Fig. 4*C*, one Mmr1-MIS^C molecule (*yellow*) adopts a conformation with an N-terminal loop (N-loop) and a C-terminal α-helix (α_{Mmr1}). The binding interface of this

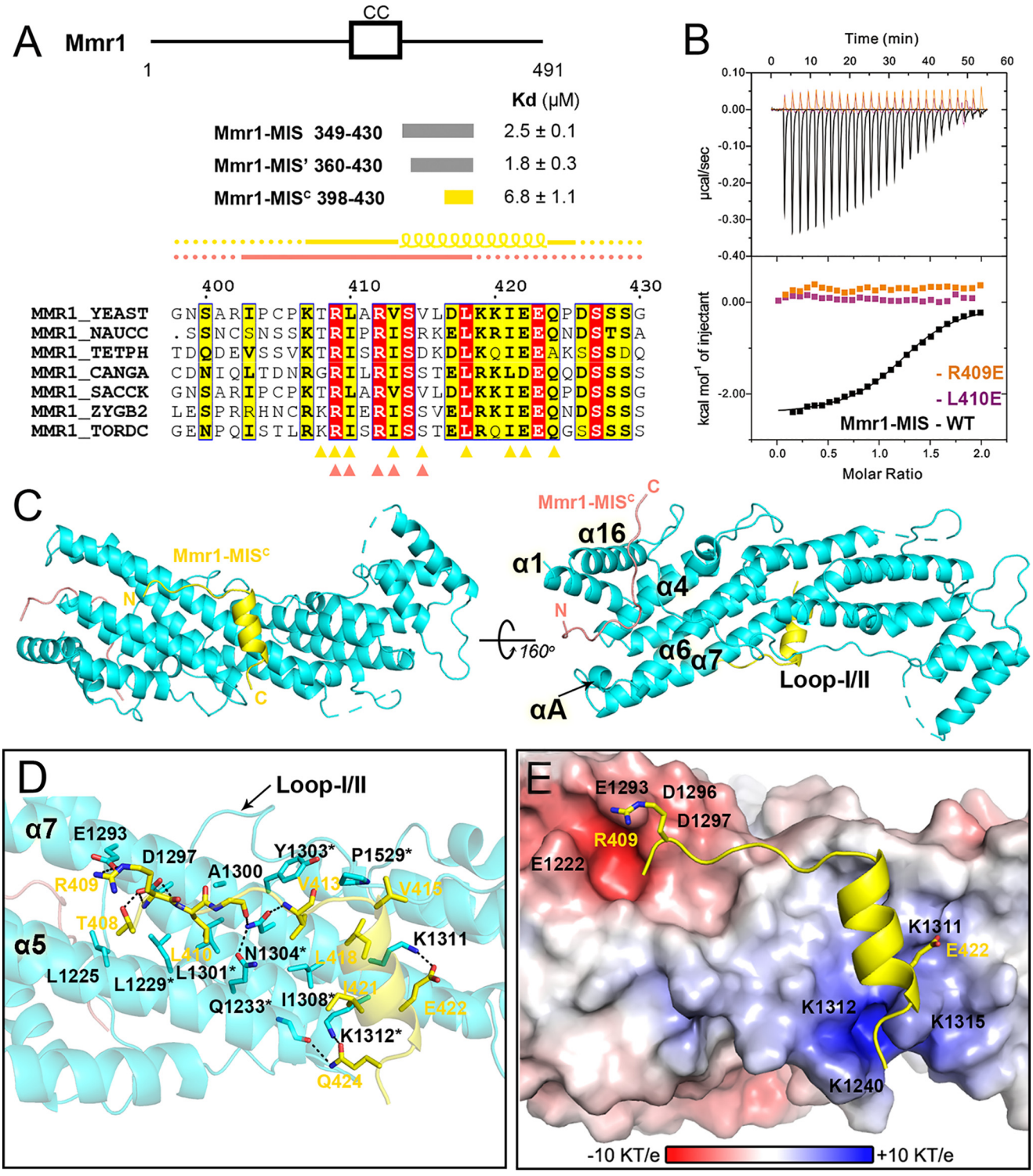

Figure 4. The Mmr1-MIS/Myo2-GTDΔL interaction. *A,* characterization of Mmr1, the Myo2 cargo adaptor for mitochondrion inheritance. The presentation style of *A* follows that of Fig. 2*A*. In the sequence alignment of Mmr1-MIS^C, an additional species was added: TETPH, *Tetrapisispora phaffii*. Residues involved in the binding of the first and second Mmr1-MIS^C molecules to Myo2-GTDΔL are indicated by *yellow* and *light pink triangles*, respectively. *B,* ITC-based analysis of the binding of Mmr1-MIS^C and its variants to Myo2-GTDΔL. *C,* the overall structure of two Mmr1-MIS^C molecules binding to GTDΔL. The color-coding is applied also in other panels of this figure. *D,* the detailed interaction between the first Mmr1-MIS^C molecule and the mitochondrion/vacuole-binding site of GTDΔL. The previously reported residues involved in the cargo binding (26) are highlighted with *stars*. *E,* the reverse charge potentials on the binding surface interact with the positively charged N terminus and the negatively charged C-terminal of the Mmr1-MIS^C peptide.

Mmr1-MIS^C molecule on Myo-GTD agrees very well with the mitochondrion/vacuole-specific binding site, as it was mapped in previous mutagenesis studies (7, 10, 14, 15, 26). More specifically, the interface includes a narrow groove between the two parallel helices, α5 and α7, for the binding of the N-loop, and a pocket formed by α5, α7, and the loop-I/II for the binding of α_{Mmr1} (Fig. 4*D* and Fig. S2). Compared with the Smy1/Inp2-binding site that is predominantly hydrophobic, this interface

on GTDΔL is much more hydrophilic. Thus, besides hydrophobic interactions, the binding of the first Mmr1-MIS^{C} molecule to GTDΔL largely depends on polar interactions. For example, N1304$_{Myo2}$ forms two strong hydrogen bonds with main chain atoms in the N-loop of Mmr1-MIS^{C}, thereby stabilizing the conformation of R412$_{Mmr1}$ for the cation-π interaction with Y1303$_{Myo2}$ (Fig. 4*D*). Interestingly, the α5/α7 groove and the α_{Mmr1}-binding pocket show reverse charge potentials, negative for the former and positive for the latter (Fig. 4*E*). Such a charge distribution on Myo2-GTD allows the specific recognition of corresponding charged residues in Mmr1-MIS^{C} by forming two charge pairs, R409$_{Mmr1}$–E1293$_{Myo2}$ and E422$_{Mmr1}$–K1311$_{Myo2}$ (Fig. 4, *D* and *E*). Considering the α_{Mmr1}-helix as a dipole, the placement of the negatively charged C-terminal end of α_{Mmr1} near the positively charged pocket of Myo2-GTD further enhances the charge–charge interaction. Together, this charge-mediated guidance is likely to play a role in orientating the Mmr1-MIS^{C} peptide to the proper position for the GTD binding. Consistent with our structural finding that both hydrophobic and charge–charge interactions are required for the Myo2/Mmr1 interaction, replacing the positively charged residue R409$_{Mmr1}$ or the hydrophobic residue L410$_{Mmr1}$ with a glutamic acid abolishes the binding of Mmr1-MIS to Myo2-GTDΔL (Fig. 4*B*).

Notably, despite the fact that E1293$_{Myo2}$ and D1297$_{Myo2}$ form salt bridges and hydrogen bonds with R409$_{Mmr1}$ and T408$_{Mmr1}$ (Fig. 4*D*), neither a E1293K nor D1297N mutant of Myo2 lost the ability to bind with Mmr1 (26). Because E1293$_{Myo2}$ and R409$_{Mmr1}$ are highly solvent exposed, the salt bridges formed between them are unlikely very stable, as indicated by the weak density of R409$_{Mmr1}$ (Fig. S4*C*). Furthermore, the charge potential change caused by the E1293K or D1297N mutation may be partially compensated by nearby negatively charged residues, like E1222$_{Myo2}$ and D1297$_{Myo2}$. Therefore, these two mutations may impair but do not eliminate the binding of Myo2 to Mmr1. Indeed, the D1297N mutant interacts with Mmr1-MIS^{C} albeit 3-fold decreased binding affinity (Table 2).

Unexpectedly, the second Mmr1-MIS^{C} molecule (Fig. 4*C*, *light pink*) binds with the Smy1/Inp2-binding groove by forming a long loop (Fig. 4, *A* and *C*, and Fig. S8*A*). Although this Mmr1-MIS^{C} molecule adopts a different conformation from Smy1-MIS^{C} and Inp2-MIS (Fig. S8*B*), two hydrophobic residues, L410$_{Mmr1}$ and V413$_{Mmr1}$, occupy a similar position to L639$_{Smy1}$ and I642$_{Smy1}$ allowing an interaction with the two hydrophobic patches, respectively (Fig. S8*A*). Furthermore, such a conformation places R409$_{Mmr1}$ in a position to form salt bridges with E1211$_{Myo2}$ (Fig. S8*A*).

The structural finding of two Mmr1-MIS^{C} molecules interacting with one GTDΔL molecule contradicts the 1:1 binding stoichiometry indicated by the biochemical data (Figs. S1*B* and S7). To test whether the Smy1/Inp2-binding groove in Myo2-GTD participates in Mmr1 binding, we measured the binding of the Smy1-MIS^{C}::GTDΔL fusion protein, and the Myo2-GTDΔL E1211A and F1275E mutants to Mmr1-MIS^{C}. In contrast to the above three designed disruptions in the Smy1/Inp2-binding groove, another four mutants on the mitochondrion/vacuole-specific binding site (D1297N, Y1303A, K1311E, and K1312A) show negligible effects on the Myo2-GTD/Mmr1-MIS^{C} interaction (Table 2), indicating that the observation of the second Mmr1-MIS^{C} molecule in the complex is likely a crystallization artifact. Nevertheless, this artifact implies that the Smy1/Inp2-binding groove has the potential to recognize cargo with different binding modes. As Mmr1 was found to compete with the vacuole-specific receptor Vac17 for binding to Myo2 (26), we tested the binding of Vac17-MIS to Myo2-GTDΔL and its mutants (Fig. S9). The Myo2 mutations on the mitochondrion/vacuole-specific binding site disrupting the Mmr1 binding were also found to interfere with the Vac17 binding. On the other hand the mutations in the Smy1/Inp2-binding site show little impact on the binding affinities (Table 2).

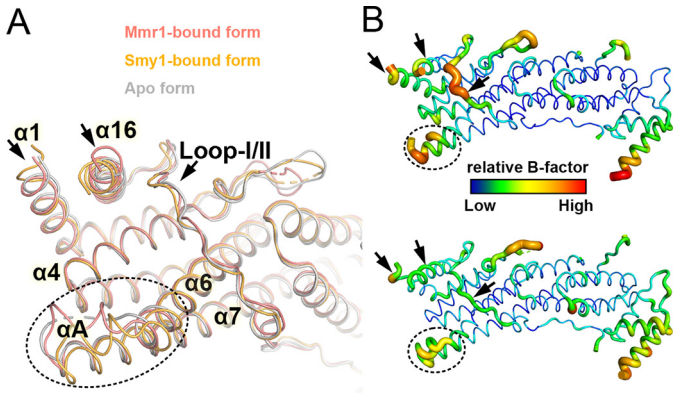

Figure 5. The high flexibility of the Smy1/Inp2-binding groove in Myo2-GTDΔL. *A,* structural comparison of Myo2-GTDΔL in apo, Mmr1-bound, and Smy1-bound form. Conformational changes are indicated by *dashed circles and arrows*. *B,* B-factor putty tube representations of Myo2-GTDΔL in apo-form (*upper panel*) and in Smy1-MIS^{C} bound form (*lower panel*). The corresponding regions highlighted in *A* are also indicated by the same elements.

The considerably higher binding affinities of Mmr1-MIS or Mmr1-MIS′ and Myo2-GTDΔL indicate that the N-terminal sequence (residues 360–397, MIS^{N}) facilitates the binding of Mmr1 to Myo2-GTDΔL. Because the N terminus of the first Mmr1-MIS^{C} molecule in the complex extends toward the Smy1/Inp2-binding groove (Fig. 4*C*), we speculated that Mmr1-MIS^{N} interacts with the groove. Consistently, both the Smy1-MIS^{C}::GTDΔL fusion and the E1211A mutation weaken the GTD binding to Mmr1-MIS′ by 2–3–fold (Fig. S7). These results suggest that Mmr1-MIS may employ the two sites to boost its binding to Myo2-GTD.

Conformational changes of the Smy1/Inp2-binding groove in Myo2-GTD for cargo binding

The overall structures of cargo-bound forms of Myo2-GTD are highly similar with that of the apo-form, except for the Smy1/Inp2-binding groove. Binding-induced conformational changes are observed in α1/α16 (the fingers), the loop-I/II, and the α6/α7 region (the thumb) (Fig. 5*A*). Specifically, the unstructured region that connects α6 and α7 forms a short αA-helix, due at least in part to the involvement of Phe-1275 in the formation of the hydrophobic patch upon cargo binding (Figs. 2*D* and 3*C*, and Fig. S8*B*). To understand the thermal motion of the Smy1/Inp2-binding groove, the distributions of B-factors (atomic displacement parameters) in the Myo2-GTDΔL structures of the cargo-free and cargo-bound forms

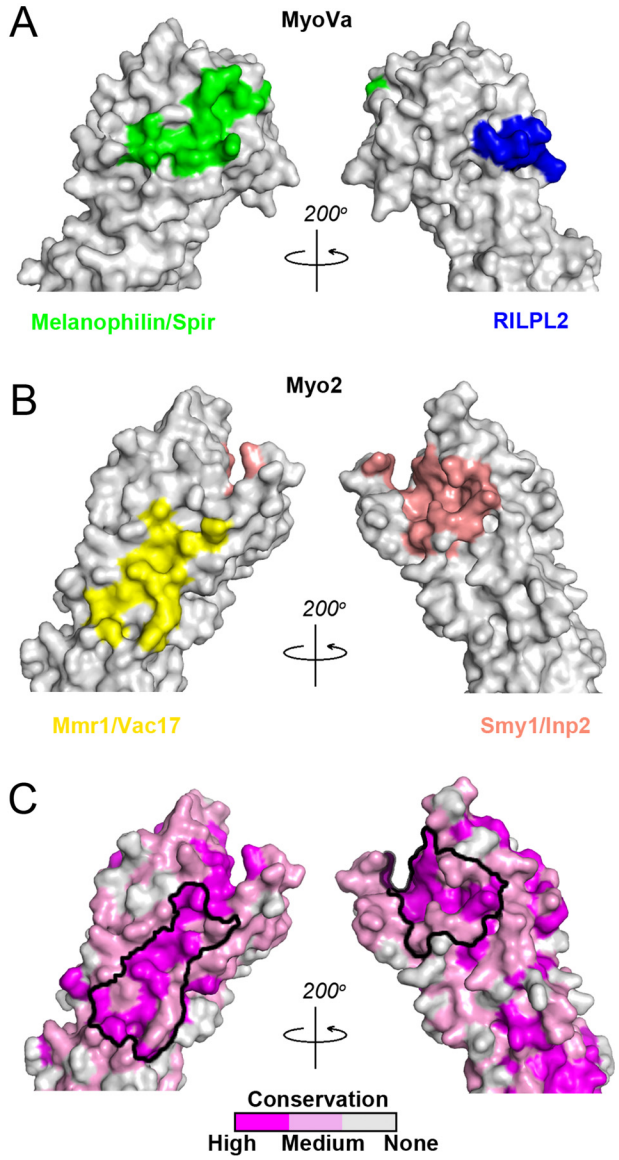

Figure 6. Surface representation of the subdomain is in Myo2-GTD and MyoVa-GTD. *A,* the previously identified cargo-binding surfaces on MyoVa (9). *B,* the binding surface on Myo2 identified in this study. *C,* surface conservation of Myo2-GTD. The indicated binding surfaces of Mmr1/Vac17-binding site and Smy1/Inp2-binding site are highly conserved.

were investigated. In general, residues in peripheral loop regions usually have higher B-factors or higher degrees of motion. However, compared with the majority of the helices, the whole Smy1/Inp2-binding groove in the apo-structure shows much stronger motion (Fig. 5*B*, *upper panel*), suggesting that the groove is highly flexible without bound cargos. Interestingly, the motion of the groove is remarkably decreased in the Smy1-bound structure (Fig. 5*B*, *lower panel*). Taken together, we propose that high flexibility is a genuine property of the Smy1/Inp2-binding groove, which can accommodate various flexible sequences in the cargo proteins to achieve the versatile binding.

An overlap of binding sites between different cargos was also found in mammalian MyoVa-GTD (9, 32). For example, the cargo adaptors Melanophilin and Spir interact with MyoVa-GTD on an identical surface (Fig. 6*A*). Compared with the Smy1/Inp2-binding site in Myo2-GTD, the Melanophilin/Spir-binding site in MyoVa-GTD shows little conformational flexibility (32). Although two different cargo-binding sites have also been identified in subdomain-I of MyoVa-GTD, they overlap only to a small extent with the cargo-binding sites of Myo2-GTD (Fig. 6, *A* and *B*). For example, the Smy1/Inp2-binding groove does not exist in MyoVa, whereas the small helix in MyoVa-GTD that is a RILPL2-binding site is replaced by a flexible loop in Myo2-GTD (Fig. 1*B*). These differences between MyoVa and Myo2 suggest that class V myosins in mammals and yeasts have evolved in very different ways to recognize their own cargos. Because the cargo adaptors of MyoVa and Myo2 share little similarity in amino acid sequences, the different cargo recognition mechanisms adopted by MyoVa and Myo2 are likely to be selected by their cargos. Nevertheless, the identified cargo-binding sites in MyoVa and Myo2 are highly conserved within vertebrates (9) and budding yeasts (Fig. 6*C*), respectively.

Discussion

Class V myosins recognize numerous cargos mainly via direct bindings of motor's GTD to cargos or cargo-specific adaptors with diverse amino acid sequences and broad physiological functions. Despite many years of extensive studies, more efforts are still required to decode the diversified yet specific recognitions by GTD. Recent progress was made mostly on mammalian class V myosins (9, 32, 33) revealing several cargo-binding modes by GTD. However, because the low sequence and structural similarity between GTDs of mammalian MyoVs and yeast Myo2 (9), those discoveries provide very limited knowledge for yeast studies. The series of structures of Myo2-GTD in complex with different cargo proteins described here advance our understanding of Myo2 function. The cargo-binding sites on Myo2-GTD described here do not only confirm previous biochemical and functional studies, but also provide key information for future *in vivo* experiments dissecting the Myo2/cargo interactions.

The structures of Myo2 in complex with Smy1 and Inp2 uncover a novel cargo-binding groove in GTD. Our structural and biochemical analysis indicates that the Smy1/Inp2-binding groove recognizes the sequence motif through conserved hydrophobic residues arranged in a specific pattern (Fig. 3*A*). The structural comparison of cargo-bound Myo2-GTD with the apo-form reveals that the Smy1/Inp2-binding groove is relatively flexible. Compared with a rigid binding surface, such a highly flexible conformation exhibiting makes the groove a versatile binding site for the MIS sequences in cargo proteins, like Smy1 and Inp2, which are largely flexible as well. Like a human hand, the flexible thumb (α6, αA, and α7), palm (α4 and the loop-I/II), and fingers (α1 and α16) work together to grasp various binding targets. Interestingly, the vesicle-binding site in subdomain-II of Myo2-GTD, which is also a versatile binding site for Ypt31/32, Sec4, and Kar9 (26), is surrounded by flexible helices and loops (Figs. 1*B* and 5*B*). It may thus be speculated that the high flexibility of the vesicle-binding site contributes to the different cargo recognitions by Myo2-GTD.

To maintain the high efficiency of Myo2-mediated cargo transport, it is very important to keep cargos associated with

the motor stably. This raises a question about the relatively low affinities measured in this work between Myo2-GTD and the MIS sequences of Smy1, Inp2, and Mmr1 (Table 2). A plausible explanation might be that these cargo adaptors contain multiple Myo2-binding sites. Consistently with this explanation, the central coiled-coil region of Smy1 was also reported to bind with Myo2 (24). Although the Inp2-binding site was mapped onto subdomain-I of Myo2-GTD in our work (Fig. 3*B*), surface residues in subdomain-II were also found to be involved in the binding of Myo2 to Inp2 (18). As the boundary used in a previous study covers a much larger region than Inp2-MIS (18), it is very likely that Inp2 interacts with Myo2-GTD by using at least two binding sites in subdomains-I and -II, respectively. Likewise, Mmr1 may also contain two Myo2-binding segments, Mmr1-MIS^{N} and -MIS^{C}, to interact, respectively, with the Smy1/Inp2-binding site and the mitochondrion/vacuole-binding site in Myo2-GTD as suggested by our findings (Fig. 4 and Fig. S7). In addition to strengthening the motor/cargo interaction, another advantage for employing a multi-binding site is to provide better regulations, beneficial for delicate control during cargo loading and unloading. For example, the binding of GTD to its cargos helps to release the head-to-tail autoinhibition (37). Because subdomain-I has been reported to participate in the head-to-tail interaction (32, 33), the cargo-binding modes identified in this study have the potential for the activation of Myo2.

We noted with interest that despite barely showing sequence similarity, the cargo adaptors including Smy1, Inp2, Mmr1, and Vac17 all contain at least one CC domain (Figs. 2*A*, 3*A*, and 4*A*, and Fig. S9). Similarly, several cargo adaptors for MyoVa, such as Melanophilin and RILPL2, also contain CCs in their sequences (9, 34). Class V myosins are known to form a dimer via their long coiled-coil domain located after the IQ repeat motifs (35, 36). Moreover, the CC domain of Melanophilins has been demonstrated to be essential for MyoVa-mediated melanosome transport in melanocytes (34). Given the possibility of CC-mediated self-association, the potential oligomerization of the cargo adaptors is likely to enhance their binding to the dimerized Myo2, and thus to increase motor's transport activity. Consistently, the dimerization of She3, an adaptor for Myo4, was found to synergistically boost the binding of She3 to Myo4 (38). A recent study demonstrated that the CC domain of Mmr1 was sufficient for self-interaction and contributed to the function in mitochondrial inheritance (31).

Experimental procedures

DNA constructs and site-directed mutagenesis

DNA encoding the GTD domain of Myo2 and the fragments of cargo adaptors were PCR-amplified from the yeast cDNA library. The coding sequences were cloned into a home-modified vector pET32a with a N-terminal thioredoxin-His$_6$ tag for protein expression and purification. All point mutations were introduced using a site-directed mutagenesis kit and confirmed by DNA sequencing.

Protein sample preparation

For the expression of the protein samples, transformed *Escherichia coli* C Plus (Novagen) were grown in LB medium at 37 °C to an optical density with $A_{600\,nm}$ of ~0.8–1.0, then induced by the addition of isopropyl 1-thio-β-D-galactopyranoside with a final concentration of 0.2 mM, and were further grown for an additional 14 h at 16 °C. The proteins were purified using Ni-affinity chromatography followed by size-exclusion chromatography with a HiLoad Superdex 200-pg 16/600 column (GE Healthcare).

ITC assay

ITC measurements were carried out on a VP-ITC Microcal calorimeter (Malvern) at 25 °C. All protein samples were dissolved in the general buffer (50 mM Tris-HCl, pH 7.5, 100 mM NaCl, 1 mM EDTA, and 2 mM DTT). Titrations were performed by injecting a protein solution containing a fragment from a cargo adaptor or its mutants at a concentration of 400 μM into a protein solution containing Myo2-GTDΔL or its mutants at a concentration of 40 μM. A time interval of 2 min between injections was used to ensure that the titration peak returned to the baseline. The titration data were analyzed using the program Origin7.0 and fitted by a one-site binding model.

Analytical gel filtration chromatography

Analytical gel filtration chromatography was carried out on an ÄKTA pure system (GE Healthcare). Protein samples at a concentration of 40 μM were loaded onto a Superdex 200 Increase 10/300 GL column (GE Healthcare), equilibrated with the general buffer.

Crystallization

To prepare the Myo2-GTDΔL/Smy1-MIS^{C} or Myo2-GTDΔL/Inp2-MIS complexes, Smy1-MIS^{C} (residues 615–650) and Inp2-MIS (531–543) were fused to the N terminus and C terminus of Myo2-GTDΔL, respectively, between a $(GS)_5$ linker and TEV cleaved site (ENLYFQS). The thioredoxin-His$_6$ tags were cleaved by HRV 3C protease at 16 °C overnight and removed by size-exclusion chromatography. The fusion proteins were concentrated to ~30 mg/ml. Prior to crystallization, TEV protease was added into the protein solutions at 4 °C overnight to cleave the fusion linkers between the cargo peptides and Myo2-GTD. To prepare the Myo2-GTDΔL/Mmr1-MIS^{C} complex, Myo2-GTDΔL and Mmr1-MIS^{C} were purified separately and then mixed in a 1:3 molar ratio to a final concentration of ~20 mg/ml. Crystallization trials were set up using the sitting drop vapor diffusion method at 16 °C. Crystals were obtained in the conditions with 1 M potassium chloride, 1 M ammonium sulfate, and 0.1 M HEPES, pH 7.0, for the Myo2-GTDΔL apo-form; 8% (w/v) PEG8000 and 0.1 M sodium dihydrogen phosphate, pH 6.5, for the Smy1-MIS^{C} bound form; 8% (w/v) PEG4000 and 0.2–0.3 M lithium/ammonium sulfate, pH 7.5, for Inp2-MIS bound form; and 20% (w/v) PEG3350 and 0.2 M sodium acetate for the Mmr1-MIS^{C} bound form. Before diffraction, the crystals were soaked in crystallization solution containing an additional 30% (v/v) glycerol for cryoprotection.

Structure determination and analysis

The X-ray diffraction datasets were collected at Shanghai Synchrotron Radiation Facility beamlines BL17U, BL18U, and BL19U1. The diffraction data were processed and scaled using

HKL2000 (39). The initial phase of the complex structure was determined by molecular replacement using the Myo2-GTD apo-structure (PDB code 2F6H) as the search model. The Mmr1 peptide was further built into the model and refined in PHENIX (40). COOT was used for model rebuilding and adjustments (41). In the final stage, an additional TLS refinement was performed in PHENIX. The model quality was checked using MolProbity (42). The model of Myo2-GTDΔL/Smy1 and Myo2-GTDΔL/Inp2 were built and refined using the same strategy as that used for the Myo2-GTDΔL/Mmr1 complex structure. Data collection and refinement statistics can be found in Table 1. The structures were deposited in the PDB with accession codes 6IXO (apo-form), 6IXQ (Smy1-MIS^C bound), 6IXR (Inp2-MIS bound), and 6IXP (Mmr1-MIS^C bound). The binding interface in the complex structures was analyzed using PISA (43). The conservation surface was generated using the Consurf server (http://consurf.tau.ac.il/2016/).[4] All structural figures were created using the PyMOL Molecular Graphics System.

Author contributions—K. T. and Y. L. data curation; K. T., Y. L., C. Y., and Z. W. formal analysis; K. T., C. Y., and Z. W. funding acquisition; K. T. and Z. W. validation; K. T., Y. L., C. Y., and Z. W. investigation; K. T. visualization; K. T., Y. L., and Z. W. methodology; K. T. and Z. W. writing-original draft; C. Y. and Z. W. resources; C. Y. and Z. W. writing-review and editing; Z. W. conceptualization; Z. W. supervision; Z. W. project administration.

Acknowledgments—We thank Dr. W. Gärtner for critical reading of the manuscript, G. Giuriani for help revising the language, the Life Science Research Center, Southern University of Science and Technology (SUSTech) for providing facilities, and the staffs from BL17U, BL18U, and BL19U1 beamlines of Shanghai Synchrotron Radiation Facility for assistance during data collection.

References

1. Hammer, J. A., 3rd, and Sellers, J. R. (2011) Walking to work: roles for class V myosins as cargo transporters. *Nat. Rev. Mol. Cell Biol.* **13,** 13–26 CrossRef Medline
2. Liu, J., Taylor, D. W., Krementsova, E. B., Trybus, K. M., and Taylor, K. A. (2006) Three-dimensional structure of the myosin V inhibited state by cryoelectron tomography. *Nature* **442,** 208–211 Medline
3. Trybus, K. M. (2008) Myosin V from head to tail. *Cell. Mol. Life Sci.* **65,** 1378–1389 CrossRef Medline
4. Fagarasanu, A., and Rachubinski, R. A. (2007) Orchestrating organelle inheritance in *Saccharomyces cerevisiae*. *Curr. Opin. Microbiol.* **10,** 528–538 CrossRef Medline
5. Heuck, A., Fetka, I., Brewer, D. N., Hüls, D., Munson, M., Jansen, R. P., and Niessing, D. (2010) The structure of the Myo4p globular tail and its function in ASH1 mRNA localization. *J. Cell Biol.* **189,** 497–510 CrossRef Medline
6. Seabra, M. C., and Coudrier, E. (2004) Rab GTPase and myosin motors in organelle motility. *Traffic* **5,** 393–399 CrossRef Medline
7. Catlett, N. L., Duex, J. E., Tang, F., and Weisman, L. S. (2000) Two distinct regions in a yeast myosin-V tail domain are required for the movement of different cargoes. *J. Cell Biol.* **150,** 513–526 CrossRef Medline
8. Schott, D., Ho, J., Pruyne, D., and Bretscher, A. (1999) The COOH-terminal domain of Myo2p, a yeast myosin V, has a direct role in secretory vesicle targeting. *J. Cell Biol.* **147,** 791–808 CrossRef Medline
9. Wei, Z., Liu, X., Yu, C., and Zhang, M. (2013) Structural basis of cargo recognitions for class V myosins. *Proc. Natl. Acad. Sci. U.S.A.* **110,** 11314–11319 CrossRef Medline
10. Pashkova, N., Jin, Y., Ramaswamy, S., and Weisman, L. S. (2006) Structural basis for myosin V discrimination between distinct cargoes. *EMBO J.* **25,** 693–700 CrossRef Medline
11. Pruyne, D., Legesse-Miller, A., Gao, L., Dong, Y., and Bretscher, A. (2004) Mechanisms of polarized growth and organelle segregation in yeast. *Annu. Rev. Cell Dev. Biol.* **20,** 559–591 CrossRef Medline
12. Itoh, T., Toh-E, A., and Matsui, Y. (2004) Mmr1p is a mitochondrial factor for Myo2p-dependent inheritance of mitochondria in the budding yeast. *EMBO J.* **23,** 2520–2530 CrossRef Medline
13. Swayne, T. C., Zhou, C., Boldogh, I. R., Charalel, J. K., McFaline-Figueroa, J. R., Thoms, S., Yang, C., Leung, G., McInnes, J., Erdmann, R., and Pon, L. A. (2011) Role for cER and Mmr1p in anchorage of mitochondria at sites of polarized surface growth in budding yeast. *Curr. Biol.* **21,** 1994–1999 CrossRef Medline
14. Ishikawa, K., Catlett, N. L., Novak, J. L., Tang, F., Nau, J. J., and Weisman, L. S. (2003) Identification of an organelle-specific myosin V receptor. *J. Cell Biol.* **160,** 887–897 CrossRef Medline
15. Tang, F., Kauffman, E. J., Novak, J. L., Nau, J. J., Catlett, N. L., and Weisman, L. S. (2003) Regulated degradation of a class V myosin receptor directs movement of the yeast vacuole. *Nature* **422,** 87–92 CrossRef Medline
16. Kumar, S., de Boer, R., and van der Klei, I. J. (2018) Yeast cells contain a heterogeneous population of peroxisomes that segregate asymmetrically during cell division. *J. Cell Sci.* **131,** jcs207522 CrossRef Medline
17. Fagarasanu, A., Fagarasanu, M., Eitzen, G. A., Aitchison, J. D., and Rachubinski, R. A. (2006) The peroxisomal membrane protein Inp2p is the peroxisome-specific receptor for the myosin V Motor Myo2p of *Saccharomyces cerevisiae*. *Dev. Cell.* **10,** 587–600 CrossRef Medline
18. Fagarasanu, A., Mast, F. D., Knoblach, B., Jin, Y., Brunner, M. J., Logan, M. R., Glover, J. N., Eitzen, G. A., Aitchison, J. D., Weisman, L. S., and Rachubinski, R. A. (2009) Myosin-driven peroxisome partitioning in *S. cerevisiae*. *J. Cell Biol.* **186,** 541–554 CrossRef Medline
19. Jin, Y., Sultana, A., Gandhi, P., Franklin, E., Hamamoto, S., Khan, A. R., Munson, M., Schekman, R., and Weisman, L. S. (2011) Myosin V transports secretory vesicles via a Rab GTPase cascade and interaction with the exocyst complex. *Dev. Cell.* **21,** 1156–1170 CrossRef Medline
20. Casavola, E. C., Catucci, A., Bielli, P., Di Pentima, A., Porcu, G., Pennestri, M., Cicero, D. O., and Ragnini-Wilson, A. (2008) Ypt32p and Mlc1p bind within the vesicle binding region of the class V myosin Myo2p globular tail domain. *Mol. Microbiol.* **67,** 1051–1066 CrossRef Medline
21. Frederick, R. L., Okamoto, K., and Shaw, J. M. (2008) Multiple pathways influence mitochondrial inheritance in budding yeast. *Genetics* **178,** 825–837 CrossRef Medline
22. Lillie, S. H., and Brown, S. S. (1992) Suppression of a myosin defect by a kinesin-related gene. *Nature* **356,** 358–361 CrossRef Medline
23. Eskin, J. A., Rankova, A., Johnston, A. B., Alioto, S. L., and Goode, B. L. (2016) Common formin-regulating sequences in Smy1 and Bud14 are required for the control of actin cable assembly *in vivo*. *Mol. Biol. Cell.* **27,** 828–837 CrossRef Medline
24. Lwin, K. M., Li, D., and Bretscher, A. (2016) Kinesin-related Smy1 enhances the Rab-dependent association of myosin-V with secretory cargo. *Mol. Biol. Cell.* **27,** 2450–2462 CrossRef Medline
25. Beningo, K. A., Lillie, S. H., and Brown, S. S. (2000) The yeast kinesin-related protein Smy1p exerts its effects on the class V myosin Myo2p via a physical interaction. *Mol. Biol. Cell.* **11,** 691–702 CrossRef Medline
26. Eves, P. T., Jin, Y., Brunner, M., and Weisman, L. S. (2012) Overlap of cargo binding sites on myosin V coordinates the inheritance of diverse cargoes. *J. Cell Biol.* **198,** 69–85 CrossRef Medline
27. Pashkova, N., Catlett, N. L., Novak, J. L., Wu, G., Lu, R., Cohen, R. E., and Weisman, L. S. (2005) Myosin V attachment to cargo requires the tight association of two functional subdomains. *J. Cell Biol.* **168,** 359–364 CrossRef Medline
28. Lillie, S. H., and Brown, S. S. (1994) Immunofluorescence localization of the unconventional myosin, Myo2p, and the putative kinesin-related pro-

[4] Please note that the JBC is not responsible for the long-term archiving and maintenance of this site or any other third party hosted site.

tein, Smy1p, to the same regions of polarized growth in *Saccharomyces cerevisiae*. *J. Cell Biol.* **125,** 825–842 CrossRef Medline

29. Hodges, A. R., Bookwalter, C. S., Krementsova, E. B., and Trybus, K. M. (2009) A nonprocessive class V myosin drives cargo processively when a kinesin-related protein is a passenger. *Curr. Biol.* **19,** 2121–2125 CrossRef Medline
30. Higuchi-Sanabria, R., Charalel, J. K., Viana, M. P., Garcia, E. J., Sing, C. N., Koenigsberg, A., Swayne, T. C., Vevea, J. D., Boldogh, I. R., Rafelski, S. M., and Pon, L. A. (2016) Mitochondrial anchorage and fusion contribute to mitochondrial inheritance and quality control in the budding yeast *Saccharomyces cerevisiae*. *Mol. Biol. Cell.* **27,** 776–787 CrossRef Medline
31. Chen, W., Ping, H. A., and Lackner, L. L. (2018) Direct membrane binding and self-interaction contribute to Mmr1 function in mitochondrial inheritance. *Mol. Biol. Cell* **29,** 2346–2357 CrossRef Medline
32. Pylypenko, O., Welz, T., Tittel, J., Kollmar, M., Chardon, F., Malherbe, G., Weiss, S., Michel, C. I., Samol-Wolf, A., Grasskamp, A. T., Hume, A., Goud, B., Baron, B., England, P., Titus, M. A., *et al*. (2016) Coordinated recruitment of spir actin nucleators and myosin V motors to rab11 vesicle membranes. *Elife* **5,** e17523 CrossRef Medline
33. Pylypenko, O., Attanda, W., Gauquelin, C., Lahmani, M., Coulibaly, D., Baron, B., Hoos, S., Titus, M. A., England, P., and Houdusse, A. M. (2013) Structural basis of myosin V Rab GTPase-dependent cargo recognition. *Proc. Natl. Acad. Sci. U.S.A.* **110,** 20443–20448 CrossRef Medline
34. Hume, A. N., Tarafder, A. K., Ramalho, J. S., Sviderskaya, E. V., and Seabra, M. C. (2006) A coiled-coil domain of melanophilin is essential for myosin Va recruitment and melanophilin transport in melanocytes. *Mol. Biol. Cell.* **17,** 4720–4735 CrossRef Medline
35. Cheney, R. E., O'Shea, M. K., Heuser, J. E., Coelho, M. V., Wolenski, J. S., Espreafico, E. M., Forscher, P., Larson, R. E., and Mooseker, M. S. (1993) Brain myosin-V is a two-headed unconventional myosin with motor activity. *Cell* **75,** 13–23 CrossRef Medline
36. Zhang, W. B., Yao, L. L., and Li, X. D. (2016) The globular tail domain of myosin-5a functions as a dimer in regulating the motor activity. *J. Biol. Chem.* **291,** 13571–13579 CrossRef Medline
37. Donovan, K. W., and Bretscher, A. (2015) Head-to-tail regulation is critical for the *in vivo* function of myosin V. *J. Cell Biol.* **209,** 359–365 CrossRef
38. Heuck, A., Du, T. G., Jellbauer, S., Richter, K., Kruse, C., Jaklin, S., Müller, M., Buchner, J., Jansen, R. P., and Niessing, D. (2007) Monomeric myosin V uses two binding regions for the assembly of stable translocation complexes. *Proc. Natl. Acad. Sci. U.S.A.* **104,** 19778–19783 CrossRef Medline
39. Otwinowski, Z., and Minor, W. (1997) Processing of x-ray diffraction data collected in oscillation mode. *Methods Enzymol.* **276,** 307–326 CrossRef Medline
40. Adams, P. D., Afonine, P. V., Bunkóczi, G., Chen, V. B., Davis, I. W., Echols, N., Headd, J. J., Hung, L.-W., Kapral, G. J., Grosse-Kunstleve, R. W., McCoy, A. J., Moriarty, N. W., Oeffner, R., Read, R. J., Richardson, D. C., *et al*. (2010) PHENIX: a comprehensive Python-based system for macromolecular structure solution. *Acta Crystallogr. D Biol. Crystallogr.* **66,** 213–221 CrossRef Medline
41. Emsley, P., and Cowtan, K. (2004) Coot: model-building tools for molecular graphics. *Acta Crystallogr. D Biol. Crystallogr.* **60,** 2126–2132 CrossRef Medline
42. Davis, I. W., Leaver-Fay, A., Chen, V. B., Block, J. N., Kapral, G. J., Wang, X., Murray, L. W., Arendall, W. B., 3rd, Snoeyink, J., Richardson, J. S., and Richardson, D. C. (2007) MolProbity: all-atom contacts and structure validation for proteins and nucleic acids. *Nucleic Acids Res.* **35,** W375–83 CrossRef Medline
43. Krissinel, E., and Henrick, K. (2007) Inference of macromolecular assemblies from crystalline state. *J. Mol. Biol.* **372,** 774–797 CrossRef Medline